Illusory Shapes via Corner Fusion

Sung Ha Kang, Wei Zhu, Jackie (Jianhong) Shen

February 27, 2014

Abstract

We propose a novel method for constructing illusory foreground and background shapes from convex corners. We first introduce a new class of visual cues called corner bases, which expands 0-dimensional corner points to 2-dimensional micro structures. These corner bases are then fused together by the functionalized elastica energy imposed upon an admissible phase field. The optimal phase field segments the visual field into disjoint connected components, which are further fused via a simple connectivity principle to construct both foreground illusory shapes and background occluded shapes. Robust and efficient numerical schemes are developed, and several generic examples are presented. Cognitive implications are highlighted.

1 Introduction

The perceptibility of illusory contours or shapes reveals the remarkable processing power of the human vision system. From the system identification point of view, illusory shapes provide an ideal class of input stimuli that help elucidate the multi-tier complex visual pathways, including for example, the feed-forward and feedback looping mechanism [45, 33].

In neurophysiology, neuronal measurements in the visual cortices of laboratory vertebrates (e.g., cats or monkeys) showed direct firing responses to illusory contours [60, 61]. On the cognitive side, vision psychologists and the gestalt school have also created numerous intriguing examples of illusory shapes or contours, reassuring the universality of illusory shape perception [31, 49]. Among them, perhaps the most well-known example is *Kanisza's Triangle* [31] (also see Figure 1, 2, and 3). In brain and neural sciences, there also has been a rich literature on the neural and neural-network foundations for illusory shapes [65, 24, 34, 56, 35].

Given such multifaceted importance in contemporary brain and cognitive sciences, many authors have striven to develop quantitative models and algorithms for illusory shapes or contours. Most classical works have relied upon feed-forward mechanisms using bottom-up artificial neural networks or local interpolation schemes (e.g., [30, 19]). A Bayesian framework potentially involving the computation at or feedback from high-tier cortical areas (e.g., V4/LOC) has been missing [43, 32].

Variational PDE models can be considered as the low-temperature limits of the Bayesian approach, and thus have witnessed increasing applications in contemporary imaging and vision sciences (e.g., the review articles [43, 10] and the monographs [3, 47, 51, 9], just to name a few). Accordingly, several authors from the variational-PDE community have revisited the challenge of modeling illusory shapes, e.g., Sarti, Malladi, and Sethian [50], Zhu and Chan [11, 66], and Jung and Shen [29]. The models in [11, 29, 50, 66] have been either image or edge based, with novel analytical concepts or computational tools such as viewpoint spread functions and active contours [50], curvatures, domain attraction, and level-set implementation [11, 66], and surface tension difference between real and illusory contours and supervision from existing shapes [29]. All these variational models work directly with the given images or the binary configurations.

The current work is based on a new class of visual cues which we call *corner bases*. A corner base is a 2-dimensional micro structure anchored at a convex corner, as to be elaborated in Sec. 2.2. Its introduction has mainly been motivated by the perceptual and cognitive significance of planer corners as illusory inducers, which is explained in Sec. 2.1. In terms of the classical literature, a corner base could be considered as a degenerate T-junction [46] when the far background and a foreground surface happen to share the same color and one shoulder of the "T" is thus muted.

Each corner base carries important local cues for the successful global reconstruction of illusory shapes. Such global fusion of local cues is facilitated by phase transition tools originated in superconductor physics [21, 40, 41], which has been popularized through numerous applications of the Γ-convergence theory in imaging and vision sciences [1, 2, 28, 36, 37, 53, 54]. To properly model the two leading factors in human's illusory perception – proximity and alignment, we employ the Γ-convergence approximations of Euler's elastica as the main phase fields to fuse the corners bases. This is to be developed in Sec. 3.

The optimal elastica phase fields fuse the scattered corner bases in the visual field into multiple connected components. These components achieve two desirable objectives. First, they bridge or fuse corners, and thus introduce a natural parity relationship or visual organization among corners. Secondly, they segment the entire region outside the given configuration into disjoint connected components. Both illusory shapes and occluded shapes are then reconstructed via a simple connectivity principle. The detailed analysis is established in Sec. 4, where we also develop a model for an associated class of intriguing illusory phenomena - ghost shapes or dots [27, 55, 20].

In Sec 5, we present all the major strategies for (i) the robust computation of the corner bases given a configuration, and (ii) the fast and efficient numerical scheme to compute the 4th order nonlinear PDE associated with the elastica phase field. Several generic examples are also presented to demonstrate the performance of the proposed model and computational schemes. In Sec 6, we consider a simplified version of our model – the total variation based corner fusion model, study the structure of its resulting sets for the decomposition of the featureless background, and especially address the formation and characterization of ghost shapes. We finally conclude the work in Sec. 7.

2 Cognitive Foundations and Corner Bases

We first address three cognitive aspects in illusory shape perception that motivate the current approach: (i) geometry vs. chromaticity, (ii) 2-D shapes vs. stand-alone contours, and (iii) the role of corners as illusory inducers. We then introduce a novel class of micro visual cues that we call corner spaces, based on which the method of phase-field fusion is developed in the next section.

2.1 Cognitive Motivations of the Current Work

Figure 1 shows different color variations of the Kanizsa Triangle displayed in panel (a). In panel (b) the gray scales of the three pacman inducers are varied, and in panel (c) three different colors are applied. In all these instances, the illusory triangles are well perceived by human observers. Such perceptual stability indicates that illusory shapes are induced mainly by the existing shapes, but not by the colors (as long as the color tones are sufficiently distinct from the background). As a result, in the current work we shall only work with a colorless layout or a *configuration* Q.

More rigorously, let Ω denote a bounded (open) image domain with Lipschitz boundaries, which corresponds to an integrated visual field, and $Q \subset \Omega$ a compact 2D domain with Lipschitz borders. For most examples of illusory shapes, one could assume that the topological boundary ∂Q consists of finitely many piecewise C^1 simply-closed curves with generic corners (i.e., no cusps [29]). In

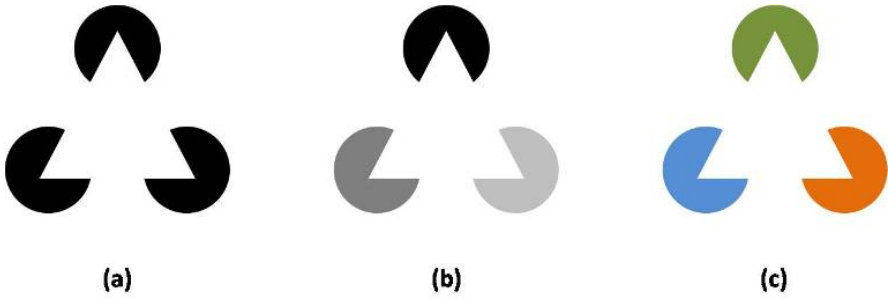

Figure 1: Perception of illusory shapes is mostly independent of the colors of the inducers (inspired by Figure 2 of Grossberg and Mingolla [25]).

terms of differential topology [12, 39], for every point along ∂Q, there is a neighborhood $U \subseteq \Omega$, which is diffeomorphic to $\mathbb{R}^2$ and $Q \cap U$ can be mapped onto either the upper half plane or the first quadrant under a diffeomorphism chart.

In Figure 2, on the other hand, we present two inducer examples either with stand-alone contours or substantially standout contours. In either scenario, the illusory triangle becomes less noticeable. It demonstrates that in order for illusory shapes to pop out robustly, the contours (with color tones) must be the topological boundaries ∂Q of a shape Q sharing the same surface tone. Since we have just shown the independence on color tones, it is further justified for us to only work with 2D configuration domains. Furthermore, the examples also imply that if there indeed exist visual cues to facilitate illusory shape perception, such cues must not be generated solely from 1D contours.

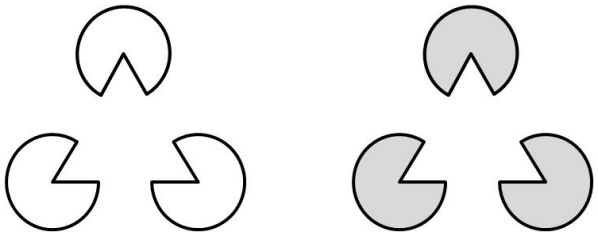

Figure 2: Stand-alone contours (left) or substantially standout contours (right) can barely induce the perception of illusory shapes (inspired by Figure 14 of Grossberg and Mingolla [25]).

Finally, corners are crucial visual cues for illusory shape, as illustrated by Figure 3. The two sets of inducers are similar, except that for the ones on the right, all corners are slightly rounded and mollified. For instance, the A2 and B2 neighborhoods on the right are the mollified versions of the A1 and B1 neighborhoods on the left which are sharp corners. The illusory shape for the rounded inducers on the right is much weaker or could not be perceived at all. Similar effects have been well documented in the literature [65, 45].

2.2 Construction of Corner Bases

With sufficient motivation and justification from the examples just discussed, we now introduce the new class of micro visual cues that we call corner bases, which serve as the cornerstones for our new model. Let Q denote the inducing configuration defined in the preceding subsection.

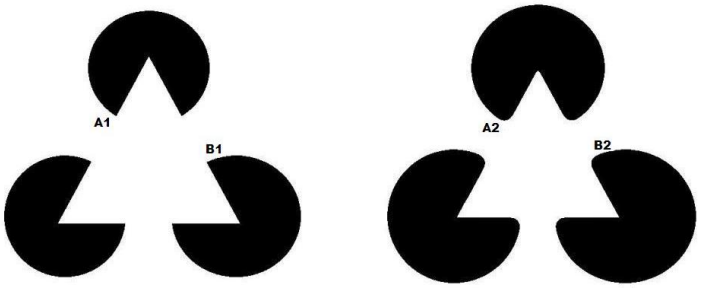

Figure 3: With sharp corners rounded, illusory shapes become much less salient.

Definition 1 *A boundary point $\boldsymbol{x} \in \partial Q$ is said to be* regular *if there is a neighborhood U of $\boldsymbol{x}$ in Ω and a C^1 invertible mapping $\Phi : U \to \mathbb{R}^2$, such that*

$$\Phi(\boldsymbol{x}) = \mathbf{0}, \quad \Phi(U) = \mathbb{R}^2, \qquad \textit{and} \quad \Phi(U \cap Q) = \mathbb{R}^1 \times (-\infty, 0].$$

The map Φ is often called a rectifying chart in differential topology [12, 15]. If $\boldsymbol{x}$ is a regular boundary point of Q, ∂Q must be a C^1 curve near $\boldsymbol{x}$. In particular, the tangent space $T_{\boldsymbol{x}}$ is well-defined. Let $\boldsymbol{n}(\boldsymbol{x})$ denote the unique unit vector which is normal to the tangent line $T_{\boldsymbol{x}}$, and points towards the exterior of Q. For simplicity, $\boldsymbol{n}(\boldsymbol{x})$ is called the outer normal of Q at $\boldsymbol{x}$.

Definition 2 (Corners) *A boundary point $\boldsymbol{c} \in \partial Q$ is said to be a* corner *if there is a neighborhood U of $\boldsymbol{c}$ in Ω and a C^1 invertible mapping $\Phi : U \to \mathbb{R}^2$, such that*

$$\Phi(\boldsymbol{c}) = \mathbf{0}, \quad \Phi(U) = \mathbb{R}^2, \qquad \textit{and} \quad \Phi(U \cap Q) = (-\infty, 0] \times (-\infty, 0]. \tag{1}$$

Furthermore, if the Jacobean $J\Phi\big|_{\boldsymbol{c}}$ at $\boldsymbol{c}$ has a positive determinant, we say that the local chart Φ is orientation preserving.

Proposition 1 *For any corner, there exists an orientation-preserving local chart Φ satisfying (1).*

Proof. If a local chart Ψ at $\boldsymbol{c}$ satisfying (1) is not orientation preserving, we have $\det(J\Psi\big|_{\boldsymbol{c}}) < 0$. Define the permutation matrix (which is also a reflection)

$$S = \begin{pmatrix} 0 & 1 \\ 1 & 0 \end{pmatrix},$$

and a new local chart Φ via composition: $\Phi = S \circ \Psi$. Then it is easy to verify that Φ must be an orientation preserving local chart at $\boldsymbol{c}$ that satisfies (1). □

Throughout the work, we assume that ∂Q is oriented so that when traveling in the orientation of ∂Q, the exterior $\Omega \setminus Q$ always lies on the right hand side. Then at any given corner point $\boldsymbol{c}$, one could define a local parametrization $\phi(s) : (-1, 1) \to \partial Q$ that satisfies:

$$\phi(0) = \boldsymbol{c}, \qquad \text{and} \quad \phi \text{ is } C^1 \text{ on both } (-1, 0] \text{ and } [0, 1),$$

and the tangent vector $\boldsymbol{t}(s) = \phi'(s)/|\phi'(s)|$ coincides with the orientation of ∂Q for any $s \neq 0$. Let $\boldsymbol{n}_-$ and $\boldsymbol{n}_+$ be the two outer normals at $\boldsymbol{c}$, such that

$$\boldsymbol{n}_- \cdot \boldsymbol{t}(0^-) = 0, \qquad \text{and} \quad \boldsymbol{n}_+ \cdot \boldsymbol{t}(0^+) = 0.$$

We refer to $\boldsymbol{n}_-$ as the pre-normal and $\boldsymbol{n}_+$ as the post-normal at the given corner.

Definition 3 (Orientation and Convexity) *Let $\boldsymbol{c}$ be a given corner of Q, and $\boldsymbol{n}_-, \boldsymbol{n}_+$ its pre- and post-normals respectively. Then the orientation $O(\boldsymbol{c})$ of the corner $\boldsymbol{c}$ is defined by*

$$O(\boldsymbol{c}) := \text{sign}(\det([\boldsymbol{n}_-, \boldsymbol{n}_+])), \qquad \textit{i.e., the sign of the determinant of the matrix } [\boldsymbol{n}_-, \boldsymbol{n}_+].$$

$\boldsymbol{c}$ is said to be convex *if $O(\boldsymbol{c}) = 1$, and* concave *if $O(\boldsymbol{c}) = -1$. The subset of all convex corners is denoted by $\angle Q$.*

The new class of micro visual cues called corner bases are defined only for convex corners. A corner base consists of two parts, the support and the corner signature.

Definition 4 (Corner Base) *Let $\boldsymbol{c} \in \angle Q$ be a convex corner with pre- and post-normal vector $\boldsymbol{n}_-$ and $\boldsymbol{n}_+$ respectively. For any $r > 0$, the r-corner base $\mathcal{B}(\boldsymbol{c}) = (D(\boldsymbol{c}), \phi_{\boldsymbol{c}})$ at $\boldsymbol{c}$ is defined as:*

(a) The support $D(\boldsymbol{c})$ is the r-disk under the given norm: $D(\boldsymbol{c}) = \{\boldsymbol{x} \ : \ \|\boldsymbol{x} - \boldsymbol{c}\| \le r\}$.

(b) The corner signature $\phi_{\boldsymbol{c}}$ is defined via

$$\phi_{\boldsymbol{c}}(\boldsymbol{x}) = \begin{cases} 0, & \boldsymbol{x} \in Q; \\ 1, & \boldsymbol{n}_- \cdot (\boldsymbol{x} - \boldsymbol{c}) \ge 0, \quad \textit{and} \quad \boldsymbol{n}_+ \cdot (\boldsymbol{x} - \boldsymbol{c}) \ge 0; \\ -1, & \textit{else.} \end{cases} \tag{2}$$

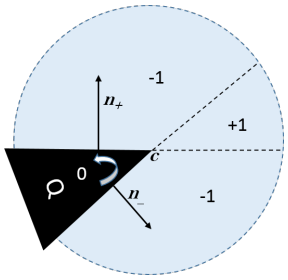

Figure 4: The pre-normal $\boldsymbol{n}_-$ and post-normal $\boldsymbol{n}_+$ at a convex corner $\boldsymbol{c}$, and the corner base supported on the shaded neighborhood $D(\boldsymbol{c})$ with different phase values for the signature $\phi_{\boldsymbol{c}}(\boldsymbol{x})$.

Figure 4 shows the definition and configuration of a typical corner base. The corner signature takes three values $\phi_{\boldsymbol{c}} : D(\boldsymbol{c}) \to \{0, -1, 1\}$. For all corner bases of a given configuration Q, we write:

$$\mathcal{B}(Q) := \mathcal{B}(\angle Q) := \{\mathcal{B}(\boldsymbol{c}) \ : \ \boldsymbol{c} \in \angle Q\}.$$

In this paper, we assume the compact set Q has a finite perimeter with a finite number of corners.

Finally we point out that the above definitions are all based on the normals, instead of the tangential vectors. This is a conscious effort embodying the priority of regions over contours, as manifested in the preceding subsection. Such an approach also leads to more robust computational schemes for computing corners or corner bases, as explained in more details in Sec. 5.1.

3 Corner Fusion via Elastica Phase Transition

For the ensemble $\mathcal{B}(Q)$ of corner bases, we present a phase-field based approach to fuse them into rudimentary regions, which will be further fused together to form visually meaningful shapes in the next section.

Definition 5 *An* ideal *phase field for a configuration Q is any function $u(\boldsymbol{x})$ of the form:*

$$u : \Omega \to \{0, +1, -1\},$$

so that $u(\boldsymbol{x}) \equiv 0$ for any $\boldsymbol{x} \in Q$, and $u(\boldsymbol{x}) \in \{-1, +1\}$ for any $\boldsymbol{x} \in \Omega \backslash Q$.

Notice that the zero phase for $u\big|_Q$ is known a priori and thus defined mostly for convenience. The distribution of the binary phases for $u\big|_{\Omega\backslash Q}$ is of the utmost interest.

Definition 6 *Given a corner base ensemble $\mathcal{B}(Q)$ of a configuration Q, an ideal phase field u is said to be admissible if*

$$u\big|_{D(\boldsymbol{c})} \equiv \phi_{\boldsymbol{c}}, \qquad \text{for any corner base} \quad \mathcal{B}(\boldsymbol{c}) = (D(\boldsymbol{c}), \phi_{\boldsymbol{c}}) \in \mathcal{B}(Q).$$

An admissible phase field u extends local corner bases to global structures, which are closely correlated to the illusory shapes being sought after. Such binary (outside Q) phase fields would be ideal for the purpose of phase extension from corner bases, but often difficult to work with both analytically and computationally. We thus instead seek continuous phase fields with sharp transitions to approximate binary ones.

Definition 7 (Diffusive Phase Field, and Admissibility) *A diffusive phase field on a visual field Ω with a configuration Q is any function $u(\boldsymbol{x})$ of the form:*

$$u\big|_Q \equiv 0, \quad \text{and} \quad u : \Omega\backslash Q \to [-1, 1] \text{ is smooth.}$$

Furthermore, given a corner-base ensemble $\mathcal{B}(Q)$ of a configuration Q, a diffusive phase field u is said to be admissible if

$$\phi_{\boldsymbol{c}} \cdot u\big|_{D(\boldsymbol{c})} \geq 0, \qquad \text{for any corner base} \quad \mathcal{B}(\boldsymbol{c}) = (D(\boldsymbol{c}), \phi_{\boldsymbol{c}}) \in \mathcal{B}(Q).$$

Without further constraints, too many phase fields would be admissible under a given ensemble of corner bases. But only few of them carry visually meaningful implications. As seen from the generic examples such as Kanizsa's Triangle, two corner bases are generally encouraged to connect when they are close and aligned well. In the language of Grenander's Pattern Theory [23], this is precisely the regularity condition for fusing the "atomic" corner bases into bigger meaningful "molecular" level structures. Such regularity conditions correspond to prior models in Bayesian visual inference [32, 43, 44]. In the variational PDE framework, they help filter out many disqualified candidates and narrow down on visually meaningful solutions.

This line of reasoning naturally invites Euler's elastica energies:

$$E(\gamma) = \int_\gamma (a + b\kappa^2) ds,$$

where κ and ds denote the curvature and arc length element along a given curve γ, and a, b are weighting costs for parting distance and orientation misalignment, reflecting the two leading factors underlying human's illusory perception. Euler's elastica was first seriously studied for visual perception and construction by David Mumford [42] in 1994. Since then, it has been frequently used as a smooth interpolator or regularizer for curves in computer vision or imaging science [38, 7], augmenting more conventional interpolators such as the cubic splines. Its functionalized version has also found broad applications in image interpolation and inpainting [7, 52].

For corner fusion, we shall also employ the functionalized elastica energy:

$$\min_u \int_{\Omega\backslash Q} \left(a + b\kappa^2(u)\right) |Du| \quad \text{with } u : \Omega\backslash Q \to [-1, 1]. \tag{3}$$

Here $\kappa(u) = \nabla \cdot (Du/|Du|)$ denotes the distributional curvature of the level surfaces of u, and $|Du|$ denotes the total variation Radon measure.

As shown in [7], working directly with the above elastica energy requires one to solve a 4th-order nonlinear geometric PDE, which is very challenging to analyze and difficult to implement. It inspires one to adopt another more friendly energy form of the elastica energy - the Γ-convergence approximation by De Giorgi [16]: $E_\epsilon(u) =$

$$\int_{\Omega\backslash Q} \left\{ a\left(\frac{\epsilon}{2}|\nabla u|^2 + \frac{W(u)}{2\epsilon}\right) + \frac{b}{\epsilon}\left(\epsilon\Delta u - \frac{W'(u)}{2\epsilon}\right)^2 \right\} d\boldsymbol{x} + \sum_{\boldsymbol{c}\in\angle Q} \int_{D(\boldsymbol{c})\backslash Q} (u - \phi_{\boldsymbol{c}})^2 d\boldsymbol{x}, \tag{4}$$

with $W(u) = (u^2 - 1)^2$ and for some bandwidth parameter ϵ close to 0. As $\epsilon \to 0^+$, the first two terms Γ-converge to the elastica energy (3) [1, 2, 14, 41, 40]. Also notice that the last term is a "softer" way to implement the ideal admissibility condition:

$$u\,|_{D(\boldsymbol{c})} \equiv \phi_{\boldsymbol{c}}, \qquad \text{for any corner base } (D(\boldsymbol{c}), \phi_{\boldsymbol{c}}) \in \mathcal{B}(Q).$$

In principle, a weight parameter could be introduced for this last term, but as far as energy minimization is concerned, it could be absorbed into the elastica cost weights a and b.

This new approximate energy is well defined in the Sobolev space $\mathcal{H}^2(\Omega\backslash Q)$. In particular, the double-well potential $W(u) = (u^2 - 1)^2$ perfectly resonates with the ideal $\{-1, 1\}$-binary phases of corner bases outside Q. The energy minimizers, which are usually non-unique due to the curvature term, provide natural fusion solutions for all the corner bases.

4 Shape Formation via Component Fusion

In previous sections, we present the importance of the (convex) corner base and merged the corner base information. Figure 5 illustrates this procedure for the classical Kanisza's Triangle. From the given configuration Q, the corner bases are shown in (b), then the new merged region $u > 0$ is shown in (c). Now $u = 0$ in Q, and either +1 or -1 on $\Omega\backslash Q$. With such partitions, we present how to reconstruct meaningful illusory objects as well as occluded background objects in this section.

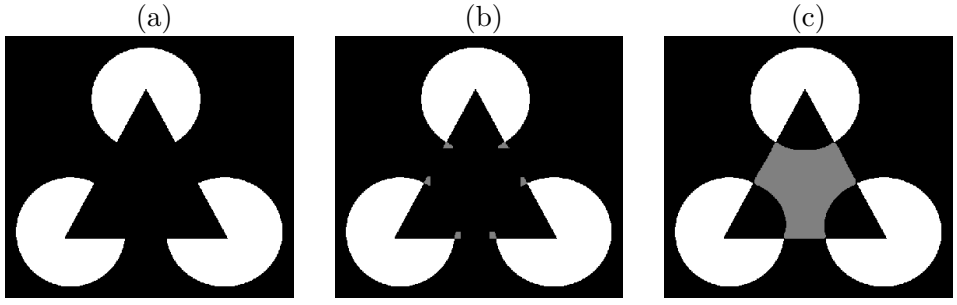

Figure 5: (a) Kanisza's Triangle; (b) Corner bases; (c) Elastica fusion with $u_* > 0$ in gray.

4.1 Structure of the Partitions

Given the elastica fusion field u_*, the original featureless background $\Omega\backslash Q$ is segmented to a *positive* region where $u_* \geq 0$ and a *negative* region R where $u_* < 0$:

$$P_* = \{\boldsymbol{x} \in \Omega\backslash Q : u_*(\boldsymbol{x}) \geq 0\}, \quad R_* = \{\boldsymbol{x} \in \Omega\backslash Q : u_*(\boldsymbol{x}) < 0\}.$$

The sets P_* and R_* include regions meeting with the image boundary $\partial\Omega$. In what follows, we use P to represent the union of connected components of P_* that don't touch the boundary $\partial\Omega$. Similarly, R denotes the interior part of R_*.

Here we make the following two assumptions:

1. $\bar{P} \subset \Omega^\circ$, the interior of the entire image domain. Here $\bar{A}$ denote its topological closure in $\mathbb{R}^2$. This assumption is to avoid the technicalities of dealing with the regions meeting with the boundary of the image domain Ω. That is we set

   $$P = \bigcup_{n=1}^{N} P_n \qquad \text{denote the decomposition of (path) connected components}$$

   where for all $n = 1, \ldots, N$, $\bar{P}_n \cap \partial\Omega = \emptyset$.

2. The optimal phase field u_* belongs to at least $C^1(\Omega\backslash Q)$, and is *non-degenerate* along the level manifold $u_* \equiv 0$ in the sense that:

   $$\nabla u_*(\boldsymbol{x}) \neq \mathbf{0}, \qquad \text{where } u_*(\boldsymbol{x}) = 0. \tag{5}$$

   This assumption is somewhat natural as it is known that the (-1)/(+1) transition profile near the zero level manifold is asymptotically the hyperbolic tanh function as $\epsilon \to 0^+$.

Similarly, we define the negative region R to be

$$R = \bigcup_{k=1}^{K} R_k, \text{ where } \bar{R}_k \cap \partial\Omega = \emptyset.$$

Therefore, among all the partition of the image domain Ω, in this paper, we only consider the partitions which does not touch the boundary of the image domain $\partial\Omega$. Figure 6, we show the region P and R for the classical Kanisza's Triangle, as derived from the elastica fusion.

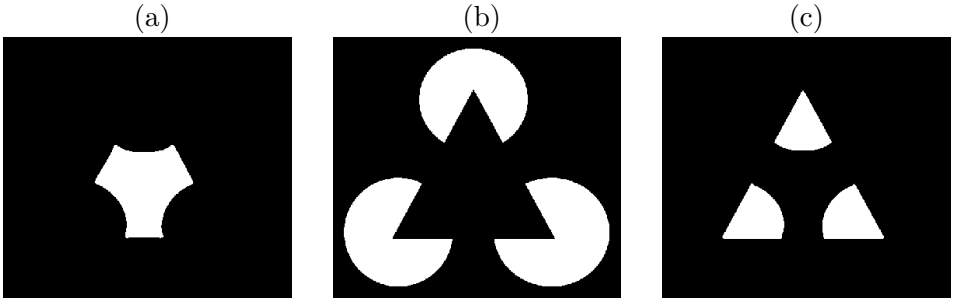

Figure 6: (a) Positive region P with $u > 0$; (b) Given Q with $u = 0$; (c) Negative region with $u < 0$.

4.2 Illusory, Occluded and Ghost Shapes

Assembling visually meaningful illusory shapes from positive or negative connected components is the process of *component fusion*. Among all the alternatives for component fusion, we have found that the following strategy is the simplest yet the most effective in approximating visual illusion.

Definition 8 (Illusory and Occluded Shapes) *Given a compact configuration Q and an optimal fusion field u_*, let P and R denote the positive and negative regions as in the preceding subsection. We then define*

$$F = P \cup R, \qquad \textit{to be the illusory foreground, and} \tag{6}$$

$$B = Q \cup R, \qquad \textit{to be the illusory background.} \tag{7}$$

Each connected component of F is said to be an illusory shape*, and each connected component of B is said to be an* occluded shape*.*

This defines the component fusion procedure that leads to the eventual reconstruction of both illusory and occluded shapes. In Figure 7 of Sec. 5.3, for example, we show the illusory and occluded shapes for the classical Kanisza's Triangle, obtained via this simple component fusion process. More generic examples will be shown in the computational section Sec. 5.

Remark 1 *Most existing works have only focused on and reconstructed the foreground illusory shapes if there are any [50, 11, 66, 29]. Our approach also naturally reconstructs the background occluded shapes.*

Remark 2 *When (foreground) illusory shapes do exist, different human observers often converge to the unique perception. However, for background occluded shapes situation can be quite different. Uniqueness should not be expected generally, because the reconstruction of background occluded shapes, given foreground shape information, becomes an inpainting problem for which non-uniqueness is intrinsic [8, 9].*

Remark 3 *Under the current component fusion method, the negative components of R bear the very simple interpretation of being the overlapping or occluding regions between the illusory foreground and background.*

The observation in the last remark inspired us to investigate further another intimately connected class of illusory perception - ghost dots or shapes, i.e., illusory shapes that pop out and disappear sporadically. Under our framework, we quantify ghost shapes as a special class of illusory shapes that have no contribution from the R components.

Definition 9 (Ghost Shape) *An illusory shape G is said to be a* ghost *shape if $G \subseteq P$. That is, there exists a positive component P_n, such that $P_n = G$.*

Ghost shapes themselves are an intriguing class of illusory phenomena, among them the Hermann Grid is the most classical example [27]. It has been traditionally held that ghost shapes emerge mainly because of the inhibitory-excitatory behavior of complex neurons [55]. The counter-example constructed by Geier et al. [20] in 2004 clearly challenged this mechanism because a small warping and smoothing of the corners can entirely mute the ghost dots which should not be the case if the above neuronal theory were true. Such fundamental roles of corners are indeed crystallized in our framework through the concepts of convex corners and corner bases.

5 Computational Methods and Examples

We first elaborate on the computational implementation of the two major components of the model: (i) construction of the corner bases, and (ii) computation of the elastica fusion field. Then we demonstrate several generic numerical examples that help illustrate the proposed model.

5.1 Robust Computation of Corner Bases

Convex corners are first of all edge points, which are defined as the difference between the configuration Q and its *eroded* version Q_e, with a numerical erosion kernel of a single-pixel radius.

To extract convex corners, at each edge point $\boldsymbol{x}$ with its local neighborhood $N_{\boldsymbol{x}}^r$ of radius r, define the *occupancy* indicator:

$$\mathrm{occup}_r(\boldsymbol{x}) := |Q \cap N_{\boldsymbol{x}}^r| / |N_{\boldsymbol{x}}^r|,$$

where $|\cdot|$ represents the 2D Lebesgue (area) measure. One has the following properties:

$$\lim_{r\to 0^+} \mathrm{occup}_r(\boldsymbol{x}) = \begin{cases} \frac{1}{2} & \boldsymbol{x} \text{ is a regular edge point,} \\ < \frac{1}{2} & \boldsymbol{x} \in \angle Q \text{ is convex,} \\ > \frac{1}{2} & \boldsymbol{x} \text{ is concave.} \end{cases}$$

Let $\theta < 1/2$ be any threshold that is numerically close to $1/2$. Then the raw convex corners are defined by

$$\angle_{\theta,r} Q = \{\boldsymbol{x} \mid \boldsymbol{x} \in \partial Q, \text{ and } \mathrm{occup}_r(\boldsymbol{x}) \le \theta\}.$$

In this paper, we assume that are finitely many convex corners. Therefore, it is easy to show that there indeed exists such a threshold $\theta < 1/2$, and some $r > 0$ such that

$$\angle Q \subseteq \angle_{\theta,r} Q.$$

To numerically extract $\angle Q$ from $\angle_{\theta,r} Q$, notice that as long as r is small enough, $\angle_{\theta,r} Q$ consists of finitely many disjoint connected components (which can also be obtained by nearest-neighbor type of clustering algorithms). For each cluster C_k, one extracts the unique convex corner via:

$$\boldsymbol{c}_k = \mathrm{argmin}_{\boldsymbol{x}\in C_k} \mathrm{occup}_r(\boldsymbol{x}).$$

All such $\boldsymbol{c}_k$'s from all the clusters give the numerical definition of the convex corner set $\angle Q$. It can be shown easily that if ∂Q is piecewise C^2, the deviation of each numerical convex corner $\boldsymbol{c}_k$ from its real location is in the order of $O(r^2)$ as $r \to 0^+$.

Next we construct the numerical corner bases. Let $f(\boldsymbol{x}) = \chi_Q(\boldsymbol{x})$ denote the characteristic function of Q. f is first slightly diffused to f_{diff} by a normal heat equation (or equivalently, smoothed by the Gaussian mollifier with suitable boundary condition). Then for any given convex corner $\boldsymbol{c} \in \angle Q$, and any $\boldsymbol{x}$ in its support $D(\boldsymbol{c})$, one computes the numerical normal vector:

$$\boldsymbol{n}_{\boldsymbol{x}} = \left(\frac{-\Delta_x f_{\text{diff}}}{\sqrt{\Delta_x f_{\text{diff}} + \Delta_y f_{\text{diff}} + \epsilon}}, \frac{-\Delta_y f_{\text{diff}}}{\sqrt{\Delta_x f_{\text{diff}} + \Delta_y f_{\text{diff}} + \epsilon}} \right),$$

via central differencing operators $\Delta_{x/y}$'s. Here the regularizer $\epsilon \ll 1$ is purely for numerical stability, and the negative sign is for the outer normals (with respect to Q). Here, to facilitate computing

over Cartesian grids, we adopted the l^∞-norm to define the support $D(\boldsymbol{c})$ of radius $r > 0$ at any convex corner $\boldsymbol{c}$:

$$\|\boldsymbol{x} - \boldsymbol{c}\|_\infty = \max\left(|x_1 - c_1|,\ |x_2 - c_2|\right), \qquad \boldsymbol{x} = (x_1, x_2),\ \boldsymbol{c} = (c_1, c_2).$$

To compute both the pre- and post-normals $\boldsymbol{n}_-$ and $\boldsymbol{n}_+$ of a given convex corner $\boldsymbol{c}$, let $\gamma = \partial Q \cap D(\boldsymbol{c})$ denote the edge set within its support. We then segment it to two segments $\gamma_\pm$ via:

$$\gamma_+ = \{\boldsymbol{x} \in \gamma \mid \det(\boldsymbol{n}_{\boldsymbol{x}}, \boldsymbol{x} - \boldsymbol{c}) > 0\}, \quad \text{and} \quad \gamma_- = \{\boldsymbol{x} \in \gamma \mid \det(\boldsymbol{n}_{\boldsymbol{x}}, \boldsymbol{x} - \boldsymbol{c}) < 0\}.$$

Let $\boldsymbol{x}_\pm$ denote the mean positions of $\gamma_\pm$. Define the weight functions via

$$w_{\boldsymbol{x}}^\pm = \exp\left(-\alpha\|\boldsymbol{x} - \boldsymbol{x}_\pm\|^2/r^2\right), \quad \text{for} \quad \pm = + \text{ or } -,$$

for some suitable decay weight $\alpha > 0$. We then define the pre- and post-normal $\boldsymbol{n}_-$ and $\boldsymbol{n}_+$ by:

$$\boldsymbol{n}_+ = \frac{\boldsymbol{n}_p}{\|\boldsymbol{n}_p\|},\ \ \boldsymbol{n}_p = \frac{\sum_{\boldsymbol{x}\in\gamma_+} w_{\boldsymbol{x}}^+ \boldsymbol{n}_{\boldsymbol{x}}}{\sum_{\boldsymbol{x}\in\gamma_+} w_{\boldsymbol{x}}^+}, \quad \text{and} \quad \boldsymbol{n}_- = \frac{\boldsymbol{n}_m}{\|\boldsymbol{n}_m\|},\ \ \boldsymbol{n}_m = \frac{\sum_{\boldsymbol{x}\in\gamma_-} w_{\boldsymbol{x}}^- \boldsymbol{n}_{\boldsymbol{x}}}{\sum_{\boldsymbol{x}\in\gamma_-} w_{\boldsymbol{x}}^-}.$$

Once the pre- and post-normals are numerically computed, the local phase function $\phi_{\boldsymbol{c}}(\boldsymbol{x})$ is then defined via (2) as in Definition 4.

5.2 Efficient Schemes for Computing Elastica Phase Fields

As addressed in Sec. 3, since direct computing of the elastica fusion field is very challenging we resort to its phase-transition approximation by De Giorgi [36, 37]:

$$E_\epsilon(u) = \int_{\Omega\setminus Q} \left\{ a\left(\frac{\epsilon}{2}|\nabla u|^2 + \frac{W(u)}{2\epsilon}\right) + \frac{b}{\epsilon}\left(\epsilon\Delta u - \frac{W'(u)}{2\epsilon}\right)^2 \right\} d\boldsymbol{x} + \int_{\Omega\setminus Q} \chi_S (u - \phi_S)^2 d\boldsymbol{x},$$

where $W(u)$ denotes the double-well potential $W(u) = (u^2 - 1)^2$, and S is the union of all the supports $D(\boldsymbol{c})$'s of corner bases outside Q (Eqn. 10). The Euler-Lagrange equation is given by

$$\begin{aligned} a\left[-\epsilon\Delta u + \frac{W'(u)}{2\epsilon}\right] + 2b\Delta\left(\epsilon\Delta u - \frac{W'(u)}{2\epsilon}\right) - \frac{b}{\epsilon^2}W''(u)\left(\epsilon\Delta u - \frac{W'(u)}{2\epsilon}\right) & \\ +2(u - \phi_S)\chi_S &= 0, \end{aligned}$$

As in the theory of Ginzburg and Landau [21] or Cahn-Hilliard [6], introduce the chemical potential:

$$v = \epsilon\Delta u - \frac{W'(u)}{2\epsilon},$$

which could also be considered as the approximate curvature field. Then the above 4th order equation could be rewritten as the a coupled system of 2nd order equations for (u, v) as in [17]:

$$\begin{aligned} 2b\Delta v - \frac{b}{\epsilon^2}W''(u)v - av + 2(u - \phi_S)\chi_S &= 0, \\ \epsilon\Delta u - \frac{W'(u)}{2\epsilon} - v &= 0, \end{aligned} \tag{8}$$

with Neumann adiabatic conditions along the boundaries [37].

In this paper, we apply Fast Fourier Transformation (FFT) to solve the above two equations via linearization and alternative iterations, as inspired by [63]. We illustrate the method via detailing on the first equation, which can be numerically expressed by:

$$-2b(\partial_1^-\partial_1^+ + \partial_2^-\partial_2^+)v + av \quad = \quad 2(u-\phi_S)\chi_S - \frac{b}{\epsilon^2}W''(u)v, \tag{9}$$

where the backward and forward differencing operators are defined via

$$\begin{aligned}
\partial_1^- v(i,j) &= \begin{cases} v(i,j) - v(i-1,j), & 1 < i \le M \ , \\ v(1,j) - v(M,j), & i = 1; \end{cases} \\
\partial_1^+ v(i,j) &= \begin{cases} v(i+1,j) - v(i,j), & 1 \le i < M-1, \\ v(1,j) - v(M,j), & i = M; \end{cases} \\
\partial_2^- v(i,j) &= \begin{cases} v(i,j) - v(i,j-1), & 1 < j \le N, \\ v(i,1) - v(i,N), & j = 1; \end{cases} \\
\partial_2^+ v(i,j) &= \begin{cases} v(i,j+1) - v(i,j), & 1 \le j < N, \\ v(i,1) - v(i,N), & j = N; \end{cases}
\end{aligned}$$

assuming that the image domain is of M by N and periodic. We then apply the discrete Fourier transform $\mathcal{F}$ to both sides of Eqn. (9). Note that

$$\begin{aligned}
\mathcal{F}\partial_1^{\pm} v(i,j) &= \pm(e^{\pm\sqrt{-1}z_i^1} - 1)\mathcal{F}v(i,j), \quad \text{and} \\
\mathcal{F}\partial_2^{\pm} v(i,j) &= \pm(e^{\pm\sqrt{-1}z_j^2} - 1)\mathcal{F}v(i,j),
\end{aligned}$$

where $z_i^1 = 2\pi(i-1)/M, i = 1, \cdots, M$, and $z_j^2 = 2\pi(j-1)/N, j = 1, \cdots, N$. Let $g = 2(u-\phi_S)\chi_S - \frac{b}{\epsilon^2}W''(u)v$ denote the term on the right hand side in Eqn. (9). At each iteration, the unknown values of u and v in g are substituted by their current iterative values, so that $g(\boldsymbol{x})$ becomes a known function. Then Eqn (9) becomes a linear equation for v at the iteration, and FFT leads to:

$$(4b(2 - \cos z_i^1 - \cos z_j^2) + a)\mathcal{F}v(i,j) = \mathcal{F}g(i,j).$$

It is easy to see that the coefficient $(4b(2-\cos z_i^1 - \cos z_j^2) + a)$ is positive, and one can thus solve for $\mathcal{F}v(i,j)$, from which v can be obtained via the inverse FFT at the current iteration. Furthermore, to be computationally more robust, one may also consider the Tikhonov type of regularization [58] of Eqn. (9):

$$-2b(\partial_1^-\partial_1^+ + \partial_2^-\partial_2^+)v + (a+c)v \quad = \quad 2(u-\phi_S)\chi_S - \frac{b}{\epsilon^2}W''(u)v + cv,$$

where the regularization constant $c > 0$ (which is often chosen to be $c = b$ in our implementation). This way even when $b \gg a$ (i.e., heavier weight on the curvature term), the numerical equation is well-posed with a good conditioning number [57, 22]. Similar numerical strategies (including regularization) are applied to the second equation for u at each iteration.

Remark 4 *There are recent advancements in using augmented Lagrangian for fast computing of curvature-based variational problems [63, 64, 67], which can be applied in these problems. We found this approach with small number of parameters was also as efficient in this case.*

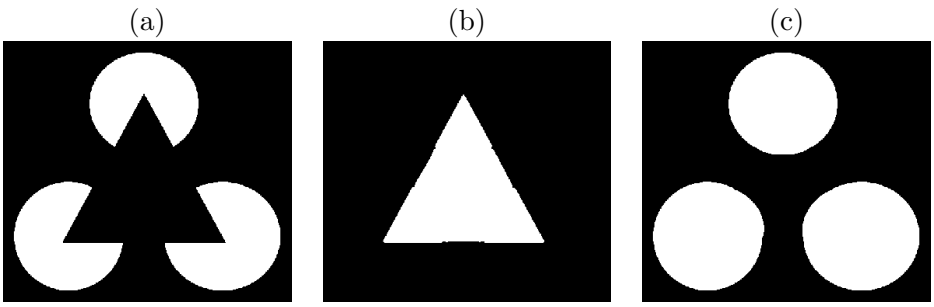

Figure 7: (a) Kanisza's Triangle; (b) Illusory shapes; and (c) Occluded shapes.

5.3 Numerical Examples

We present several generic numerical examples in this section. Figure 7 reproduces the classical example of Kanisza's Triangle. Most existing models only produce the illusory shapes [50, 11, 29]. The current approach also reconstructs the occluded shapes, or at least one candidate solution. Generally as intrinsic for inpainting [7, 8, 52], occluded shapes are not unique.

In Figure 8 and 9, we present two generic examples with more complex configurations. The optimal fusion fields are able to make blind fusion for the complex layouts of corner bases, and to reconstruct illusory shapes that are consonant with human's illusory perception. We emphasize again that occluded shapes are generally not unique and that the model offers a plausible candidate.

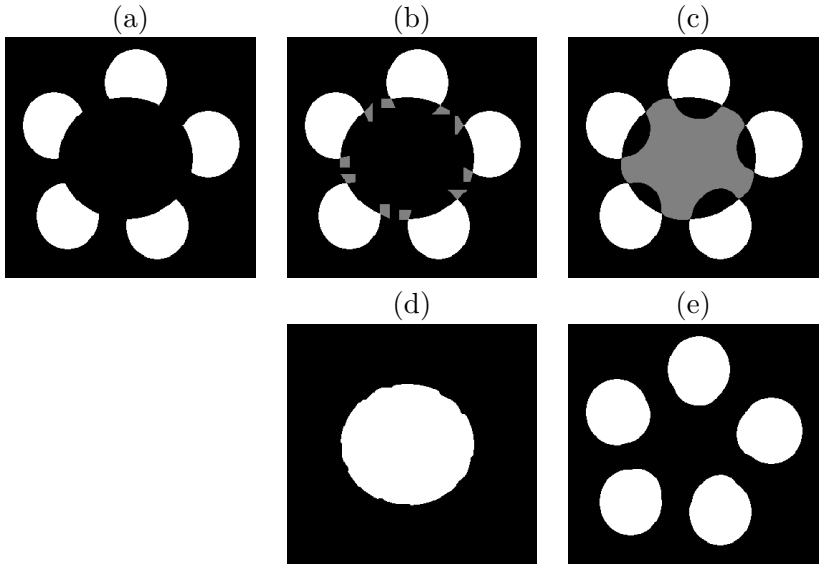

Figure 8: (a) Q; (b) corner bases in gray; (b) Elastica fusion field in gray; (c) Illusory shape; (d) Occluded shapes.

Figure 10 demonstrates an example of ghost shapes. The illusory shape itself is a positive component and thus is a ghost shape by Definition 9. This particular example could be seen as one period of the periodic inducer in the Hermann Grid [27] which is the most orthodox example for the illusory phenomenon of ghost shapes. The conventional interpretation has been based on the inhibitory skirting of a ganglion cell at the early stage of the visual pathway [55]. But this view

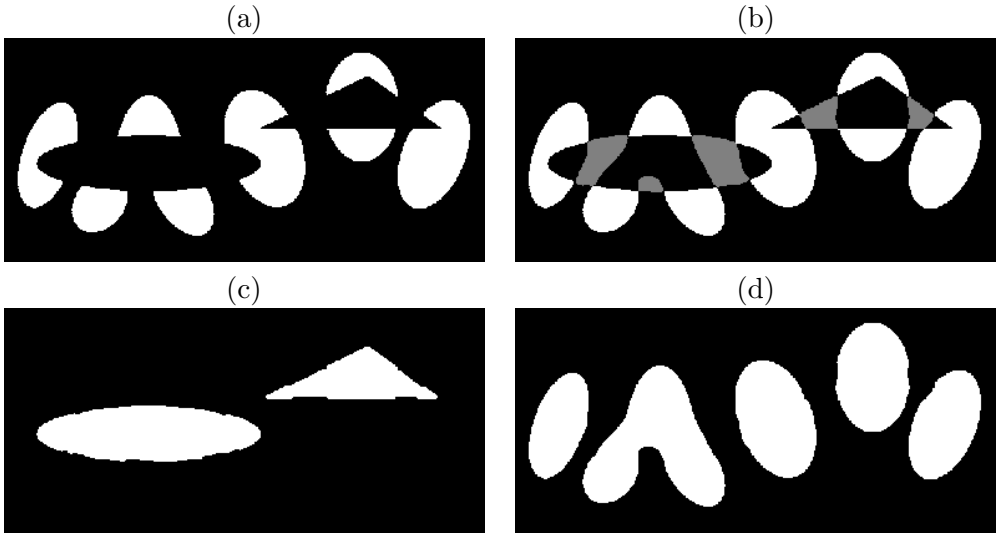

Figure 9: (a) Configuration Q; (b) Elastica fusion field; (c) Illusory shapes; (d) Occluded shapes.

has been contested by the counterexample constructed by Geier et al. [20], where a small warping perturbation has got rid of the ghost shapes while theoretically it should not if the inhibitory theory were correct. Our model is consistent with the example of Geier et al. as it has been explicitly developed from the corner bases, which also disappear after any smooth warping.

Under our framework, we conjecture that the ghostness (i.e., transient emergence to human vision) is due to lack of the surrounding negative region R, which represents the occlusion of background shapes by foreground illusory shapes. Such lack of occluding evidences or hints makes the perception of the foreground illusory shapes unstable. In the feed-forward/feedback, or equivalently, the bottom-up/top-down framework of vision [33, 26, 62], we further conjecture that the emergence of ghost shapes is due to the feed-forward computing in areas such as V1/V2, while their dissolution is due to the feedback supervision from higher-tier areas such as V4/LOC [45] which signals the lack of occluding evidences and hence rebuts the feed-forward null hypothesis on the existence of illusory shapes. The neuro-physiological evidences for the involvement of higher-tier areas (in particular, LOC) in the perception of illusory shapes can be found in [56, 35].

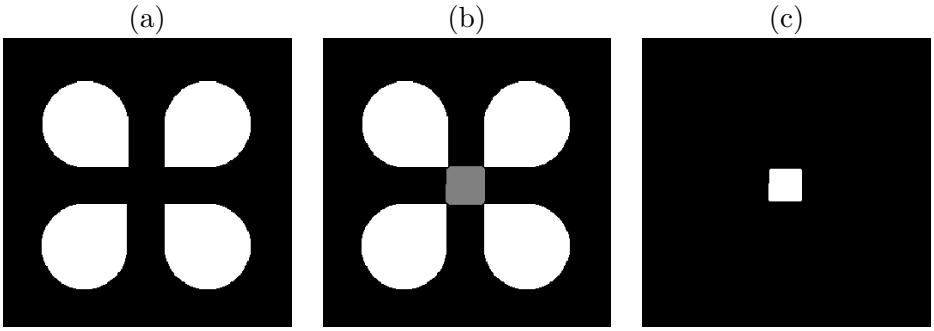

Figure 10: (a) Configuration Q; (b) Fusion field; (c) Illusory shapes. By Definition 9, the illusory square is a ghost shape. This example can be seen as one period of the periodic inducer in the famous Hermann Grid [27].

6 Analysis on the Total Variation based Model

In this section, we discuss some theoretical properties of the proposed fusion model when $b = 0$, i.e., the case of total variation (TV) based corner fusion. Analysis for elastica fusion is much more involved due to the nonlinear curvature term. Here we note that Bellettini and March [5] and Coscia [13] considered theory/analytical aspects of curvature based variational models to related problems. For example, in [5], the authors considered the problem of segmentation with depth, and studied the characteristics of minimizing segmentation considering the occluded boundaries and depth order. These connections will be explored in future work. Although the following analysis is for a simplified model, it expands to discussion of ghost shapes, and gives a good insight and general direction for the future studies.

In this section, we assume the given configuration Q has the object boundaries to be either strictly consists of piecewise straight lines or straight level lines close to each $D(\boldsymbol{c})$, that the reconstruction is only assumed to be a combinations of piecewise straight linear lines. This is to be consistent with TV base reconstruction.

Define the total supervised region $S \subseteq \Omega \backslash Q$ from all corner bases:

$$S = \bigcup_{\boldsymbol{c} \in \angle Q} \left(D(\boldsymbol{c}) \setminus Q \right), \tag{10}$$

and total supervised function $\phi_S(\boldsymbol{x})$ for $\boldsymbol{x} \in \Omega \setminus Q$ from the individual signatures:

$$\phi_S(\boldsymbol{x}) = \phi_{\boldsymbol{c}}(\boldsymbol{x}), \text{ for } \boldsymbol{x} \in D(\boldsymbol{c}) \text{ for some } \boldsymbol{c} \in \angle Q \; ; \qquad \phi_S(\boldsymbol{x}) = -1, \text{ otherwise.}$$

For $b = 0$, the fusion energy (4) becomes:

$$E_\epsilon(u) = a \int_{\Omega \backslash Q} \left(\frac{\epsilon}{2} |\nabla u|^2 + \frac{W(u)}{2\epsilon} \right) d\boldsymbol{x} + \int_{\Omega \backslash Q} \chi_S \cdot (u - \phi_S)^2 d\boldsymbol{x}, \tag{11}$$

where $\chi_S = \chi_S(\boldsymbol{x})$ denotes the characteristic function of S.

Theorem 1 *Assume that the complement $\Omega \backslash Q$ of a given configuration Q is a bounded Lipschitz domain. Then for any parameter $a > 0$, $\epsilon > 0$, the minimizer to the energy $E_\epsilon(u)$ in Eqn. (11) exists in the Sobolev space of:*

$$\mathcal{H}^1(\Omega \setminus Q, [-1, 1]) = \{ u \in \mathcal{H}^1(\Omega \setminus Q) : \; u \in [-1, 1] \}.$$

The proof is somewhat standard and hence omitted here, after having the following facts observed: (i) the illusion-free phase field $u_f(\boldsymbol{x}) \equiv -1$ is admissible, and (ii) the complement $\Omega \backslash Q$ is bounded, and the double-well $W(u)$ is Lipschitz over $u \in [-1, 1]$. Notice that uniqueness is generally not guaranteed due to the non-convexity of the double-well potential.

As stated earlier, the transition from binary phases to diffusive phase fields carries more advantages for modeling and computation. It is still interesting to investigate the ideal binary phase fields in the framework of bounded variations (BV). We use the ordinary Euclidean norm for defining the supports $D(\boldsymbol{c})$'s of corner bases.

Theorem 2 *Assume the complement $\Omega \backslash Q$ of a given configuration Q is a bounded Lipschitz domain. Then for any cost parameter $a > 0$, the minimizer to the ideal BV fusion energy $E_{\mathrm{BV}}(u)$*

$$E_{\mathrm{BV}}(u) = a \int_{\Omega \backslash Q} |Du| + \int_{\Omega \backslash Q} \chi_S \cdot (u - \phi_S)^2 d\boldsymbol{x}$$

exists in the restricted binary BV space of:

$$\mathrm{BV}_{bin}(\Omega \setminus Q) = \{u \in \mathrm{BV}(\Omega \setminus Q) : \ u(\boldsymbol{x}) = 1 \ or \ -1, \ \ \boldsymbol{x} \in \Omega \setminus Q\}.$$

Furthermore, for any such minimizer u_*:

$$E_{\mathrm{BV}}(u_*) \leq 2ar(2+\pi) \cdot \#(\angle Q),$$

where $\#(\angle Q)$ counts the number of convex corners, and r is the radius for each corner base.

Proof. First, $u_0 = \phi_S$ clearly belongs to $\mathrm{BV}_{bin}(\Omega \setminus Q)$, and by the co-area formula,

$$\begin{aligned} E_{\mathrm{BV}}(u_0) &= a \int_{\Omega \setminus Q} |Du_0| = a \int_{-1}^{1} d\lambda \int_{\Omega \setminus Q} \left| D\chi_{(u_0 < \lambda)} \right| \\ &\leq a \cdot 2 \cdot \#(\angle Q) \cdot (r + r + \pi r) = 2ar(2+\pi) \cdot \#(\angle Q). \end{aligned}$$

Here the circumference of the region with $+1$ on a corner base consists of the two radii plus the circular arc in between, which is less than πr due to convexity. Therefore, the upper bound holds for any minimizer u_*.

The main approach to establishing existence can be found in several related works (e.g., Vese et al. [4, 59]), which we now explain. Let $(u_n \mid n = 1, 2, \cdots)$ be a minimizing sequence. Due to the boundedness of both $\|u_n\|_{L^\infty(\Omega \setminus Q)}$ and $\displaystyle\int_{\Omega \setminus Q} |Du_n|$, and the pre-compactness of $\mathrm{BV}(\Omega \setminus Q)$ in $L^1(\Omega \setminus Q)$, there can be found a subsequence $(v_k \mid k = 1, 2, \cdots)$ and some $u_* \in L^1(\Omega \setminus Q)$, such that v_k converges to u_* in $L^1(\Omega \setminus Q)$. Due to the L^∞-boundedness of the subsequence, the convergence holds even in L^2. Therefore,

$$\int_{\Omega \setminus Q} \chi_S (u_* - \phi_S)^2 d\boldsymbol{x} = \int_S (u_* - \phi_S)^2 d\boldsymbol{x} = \lim_{k \to \infty} \int_S (v_k - \phi_S)^2 d\boldsymbol{x} = \lim_{k \to \infty} \int_{\Omega \setminus Q} \chi_S (v_k - \phi_S)^2 d\boldsymbol{x}.$$

Then the lower semi-continuity of the TV Radon measure ensures

$$E_{\mathrm{BV}}(u_*) \leq \liminf_{k \to \infty} E_{\mathrm{BV}}(v_k) = \inf_{u \in \mathrm{BV}_{bin}(\Omega \setminus Q)} E_{\mathrm{BV}}(u).$$

To show u_* is a minimizer, pick a subsequence v_k converging to u_* almost everywhere (a.e.). Since each v_k is (-1)/(+1) binary, the a.e. convergence implies that u_* must be (-1)/(+1) binary as well. This concludes the proof. □

As in the TV inpainting model proposed by Chan and Shen [8], uniqueness is generally not guaranteed, due to the lack of strict convexity. TV is very different from other smoother interpolators such as splines or Sobolev functions. In particular, the upper bound established in Theorem 2 only applies to the global minimum, and visually meaningful local optima may well break such barriers. See [8] for more discussion.

6.1 Structure of Positive Components

For each convex corner $\boldsymbol{c} \in \angle Q$, define the positive-phase area $D_+(\boldsymbol{c})$ via

$$D_+(\boldsymbol{c}) = \{\boldsymbol{x} \in D(\boldsymbol{c}) : \phi_{\boldsymbol{c}}(\boldsymbol{x}) = +1\}.$$

From now, we assume that the optimal phase field u_* is admissible: $u_* \cdot \phi_{\boldsymbol{c}} \geq 0$ on any corner support $D(\boldsymbol{c})$ with $\boldsymbol{c} \in \angle Q$.

Lemma 1 *If for some n and $\boldsymbol{c} \in \angle Q$, $P_n \cap D_+(\boldsymbol{c}) \neq \emptyset$, then we must have $D_+(\boldsymbol{c}) \subseteq P_n$.*

Proof. Due to the admissible assumption $u_* \cdot \phi_c \geq 0$ on $D(\boldsymbol{c})$, we have $u_* \geq 0$ on $D_+(\boldsymbol{c})$ and thus $D_+(\boldsymbol{c}) \subseteq P$. Since $D_+(\boldsymbol{c})$ itself is connected, there must exist some m such that $D_+(\boldsymbol{c}) \subseteq P_m$. Since any two different connected components must be disjoint, we must have $P_m = P_n$. □

Proposition 2 *For any convex corner $\boldsymbol{c} \in \angle Q$, there is one and only one connected component P_n, such that $\boldsymbol{c} \in \bar{P}_n$.*

Proof. By the preceding lemma, for any corner $\boldsymbol{c} \in \angle Q$, there is one and only one connected component P_n, such that $D_+(\boldsymbol{c}) \subseteq P_n$. Then $\boldsymbol{c} \in \bar{P}_n$. By the definition of the corner signature function $\phi_{\boldsymbol{c}}$, we must have

$$(D(\boldsymbol{c}) \setminus D_+(\boldsymbol{c})) \cap P = \emptyset, \quad \text{and consequently,} \quad D(\boldsymbol{c}) \cap P_m = \emptyset, \quad m \neq n.$$

Since $D(\boldsymbol{c})$ is a topological neighborhood of $\boldsymbol{c}$ in $\mathbb{R}^2$, one has $\boldsymbol{c} \notin \bar{P}_m$ for any $m \neq n$. Therefore, P_n is the only one component whose topological closure contains $\boldsymbol{c}$. □

Next we show that the opposite association rule is also true.

Proposition 3 *For any connected component P_n, there exists at least one convex corner $\boldsymbol{c} \in \angle Q$, such that $\boldsymbol{c} \in \bar{P}_n$.*

Proof. Suppose there exists a number of connected component P_n such that $\angle Q \cap \bar{P}_n = \emptyset$. Then by Lemma 1, we must have:

$$P_n \cap S = \emptyset, \qquad S \text{ as defined in Eqn. (10).}$$

To avoid being distracted by boundary complications and micro-structure details of optimal solutions, here we only consider the case when $P_n \subseteq \Omega \backslash Q$ is compact. Since S is relatively closed in $\Omega \backslash Q$, there exist some $\delta > 0$ and a neighborhood $P_{n,\delta}$, such that

$$P_{n,\delta} \cap S = \emptyset, \quad P_{n,\delta} \subset \Omega \backslash Q, \quad \text{with } P_{n,\delta} = \{\boldsymbol{x} \in \mathbb{R}^2 : dist(\boldsymbol{x}, P_n) < \delta\}.$$

By the definitions of P and P_n, we must have

$$u_*(\boldsymbol{x}) = 0, \qquad \boldsymbol{x} \in \partial P_n.$$

Due to the non-degeneracy assumption in Eqn. (5), ∂P_n is a 1-D embedded manifold with at least C^1 smoothness. By the Implicit Function Theorem, as long as $\delta > 0$ is small enough, there must exist some $m_\delta > 0$, such that for any positive $m < \min(m_\delta, 1)$,

$$P_n^m = \{\boldsymbol{x} \in P_{n,\delta} : u_*(\boldsymbol{x}) \geq -m\},$$

is a connected compact manifold with C^1 border ∂P_n^m, on which $u_* \equiv -m$. We fix the pair of δ and m below.

We construct a new phase function $u_\triangle \in \mathcal{H}^1(\Omega \backslash Q, [-1, 1])$:

$$u_\triangle(\boldsymbol{x}) = \begin{cases} u_*(\boldsymbol{x}) & \text{if } \boldsymbol{x} \in (\Omega \backslash Q) \setminus P_n^m; \\ -m & \text{if } \boldsymbol{x} \in P_n^m \text{ and } u_*(\boldsymbol{x}) \in [-m, m]; \\ -u_*(\boldsymbol{x}) & \text{if } \boldsymbol{x} \in P_n^m \text{ and } u_*(\boldsymbol{x}) > m. \end{cases}$$

Since $P_n^m \subset P_{n,\delta}$, and $P_{n,\delta} \cap S = \emptyset$, we have $S \subseteq (\Omega \backslash Q) \setminus P_n^m$ and $u_\triangle \equiv u_*$ on S, and

$$\int_{\Omega\backslash Q} \chi_S (u_\triangle - \phi_S)^2 d\boldsymbol{x} = \int_S (u_\triangle - \phi_S)^2 d\boldsymbol{x} = \int_S (u_* - \phi_S)^2 d\boldsymbol{x} = \int_{\Omega\backslash Q} \chi_S (u_* - \phi_S)^2 d\boldsymbol{x}. \tag{12}$$

And, the construction of the new phase field ensures that $W(u_\triangle) \leq W(u_*)$ since (i) $W(\cdot)$ is an even function, and (ii) $W(-m) \leq W(u)$, for any $u \in [-m, m]$, and the strict inequality holds for any $u \in (-m, m)$. Therefore, one must have

$$\int_{\Omega\backslash Q} W(u_\triangle) d\boldsymbol{x} < \int_{\Omega\backslash Q} W(u_*) d\boldsymbol{x}. \tag{13}$$

Here the strict inequality holds by the construction of P_n^m, the set

$$G = P_n^m \cap \{\boldsymbol{x} \in \Omega\backslash Q : u_*(\boldsymbol{x}) \in (-m, m)\}$$

have a non-empty interior (since $u_* \geq 0$ on $P_n \subset P_n^m$, $u_* = -m$ on ∂P_n^m, and P_n^m is connected), thus a positive Lebesgue measure. On this set one has $W(u_\triangle(\boldsymbol{x})) \equiv W(-m) < W(u_*(\boldsymbol{x}))$. Similarly, on this set one has: $\int_G |\nabla u_\triangle|^2 d\boldsymbol{x} = 0 < \int_G |\nabla u_*|^2 d\boldsymbol{x}$. Then by the definition of $u_\triangle$,

$$\int_{\Omega\backslash Q} |\nabla u_\triangle|^2 d\boldsymbol{x} < \int_{\Omega\backslash Q} |\nabla u_*|^2 d\boldsymbol{x}. \tag{14}$$

Using the equations (12), (13), (14), $E_\epsilon(u_\triangle) < E_\epsilon(u_*)$. Since $u_\triangle \in \mathcal{H}^1(\Omega\backslash Q, [-1, 1])$, this contradicts to u_* being an optimal fusion phase. □

These two propositions give the key implication for the following.

Theorem 3 *Given a configuration Q with finitely many convex corners, all the positive connected components of P_* naturally induce a complete partition of the corner set $\angle Q$, with the closure of each component $\bar{P}_n$ containing a unique non-empty subset of $\angle Q$. In particular, the number N of positive connected components must satisfy:*

$$N = \#\textit{positive connected components} \leq \#(\angle Q) < \infty.$$

6.2 Structure of Negative Components

Given an optimal fusion phase u_*, one can further define the *negative* area to be:

$$R_* = \{\boldsymbol{x} \in \Omega\backslash Q : u_*(\boldsymbol{x}) < 0\} = R_0 \cup R,$$

where R_0 denotes the union of connected components that meet the domain boundary $\partial\Omega$, and R the union of all other interior connected components as defined earlier, i.e., R_0 and R are disjoint, and

$$R_0 = \bigcup_{m=1}^{M} R_{0,m}, \qquad R = \bigcup_{k=1}^{K} R_k,$$

here $R_{0,m}$'s and R_k's are disjoint connected components of R, and

$$\bar{R}_k \cap \partial\Omega = \emptyset, \qquad \bar{R}_{0,m} \cap \partial\Omega \neq \emptyset.$$

For convenience, we refer to R_0 as the *far* background. Similar to the case of positive components, one has the following for the negative components.

Theorem 4 *(i) For each convex corner $\boldsymbol{c} \in \angle Q$, there is at least one and at most two negative connected components of R whose closure in $\mathbb{R}^2$ contains $\boldsymbol{c}$. (ii) For each connected component of R, there is at least one convex corner $\boldsymbol{c} \in \angle Q$ included in its closure in $\mathbb{R}^2$. (iii) Let $N = \#\angle Q$ denote the total number of convex corners. Then $M + K \leq 2N$.*

6.3 Ghost Shapes

In this section, we further proceed with the study of ghost shapes using the energy $E_\epsilon(\cdot)$ in (11) with the piecewise linear straight line boundary configuration Q. We introduce the concept of ghost corners at the post fusion stage.

Definition 10 (Ghost Corner) *A convex corner $\boldsymbol{c} \in \angle Q$ is said to be a* ghost corner *if*

$$D(\boldsymbol{c}) \setminus (P_n \cup Q) \subset R_0, \quad \textit{i.e., contained in the far background,}$$

assuming that P_n is the unique positive component such that $\boldsymbol{c} \in \bar{P}_n$ (see Proposition 2).

Lemma 2 *Let u_* be the optimal fusion phase for E_ϵ in Eqn. (11). Assume it is non-degenerate in the sense of Eqn. (5) along its zero level manifold $\Gamma = \{\boldsymbol{x} \in \Omega \backslash Q : u_*(\boldsymbol{x}) = 0\}$. Then Γ cannot have any compact connected component.*

We only outline the proof here: First, any compact connected component $\gamma \subseteq \Gamma$ must not intersect with any corner base $D(\boldsymbol{c})$ for some $\boldsymbol{c} \in \angle Q$ since that would imply such a $\boldsymbol{c}$ belongs to $\bar{\gamma}$ but not to γ. This contradicts to the compactness and hence closedness of γ. Secondly, by the non-degeneracy condition, any compact connected component γ must be a 1-D manifold embedded in $\mathbb{R}^2$ (that is actually diffeomorphic to the canonical circle). Therefore, one can define a slightly perturbed new admissible phase field $u_\triangle$ from u_* to produce a slightly perturbed new admissible phase field $u_\triangle$, as in the proof of Proposition 3. This is localized in the neighborhood of γ, so that (i) there will be no change of the fitting energy term over S in $E_\epsilon(\cdot)$ since $\gamma \cap S = \emptyset$; and (ii) γ is slightly contracted or morphed to a new 1-D manifold $\tilde{\gamma}$ which has strictly shorter length (i.e., via mean-curvature type of motion [48, 51, 18]). Since for small ϵ the regularized double-well energy term in $E_\epsilon(\cdot)$ Γ-converges to the length of the 1-D manifold Γ, one has $E_\epsilon(u_\triangle) < E_\epsilon(u_*)$ after some asymptotic argument, which contradicts to the assumption on u_*.

The next result characterizes global ghost shapes completely via local ghost corners.

Theorem 5 *Suppose that the trace of an optimal fusion u_* along ∂Q is -1. Then a positive component P_n is a ghost shape if and only if all convex corners in $\bar{P}_n \cap \angle Q$ are ghost corners.*

Proof. ($\Leftarrow$) Suppose all convex corners in $\bar{P}_n \cap \angle Q$ are ghost corners. If P_n is not a ghost shape, then this is an illusory shape A, such that $P_n \subset A$, and A contains at least one non-boundary negative component. Since all positive components are disjoint by definition, there must exist at least one non-boundary negative component $R_k \subset A$ with $k \geq 1$, such that $\bar{R}_k \cap \bar{P}_n \neq \emptyset$ and $\Gamma_{nk} = \partial R_k \cap \partial P_n \neq \emptyset$. Due to the non-degeneracy assumption, Γ_{nk} is a locally 1-D embedded manifold on $\Omega \backslash Q$. By Lemma 2, Γ_{nk} cannot have any compact connected component within the open domain $\Omega \backslash Q$. Then Γ_{nk} must have at least one connected component, say γ, that intersects with ∂Q. Notice that

$$\gamma \cap \partial Q \subseteq \Gamma_{nk} \cap \partial Q \subseteq \angle Q, \quad \text{since by the assumption, } u_*\big|_{\partial Q} = -1, \text{ a.e.}$$

Thus γ contains at least one convex corner, say, $\boldsymbol{c} \in \angle Q$. Since $\gamma \subseteq \partial R_k \cap \partial P_n$, this implies that $\boldsymbol{c} \in \bar{P}_n$, and

$$(D(\boldsymbol{c}) \backslash (P_n \cup Q)) \cap R_k \neq \emptyset.$$

This contradicts that $\boldsymbol{c} \in P_n \cap \angle Q$ must be a ghost corner, so that $D(\boldsymbol{c}) \backslash (P_n \cup Q)$ is completely contained in the far background R_0, which is disjoint with R_k.

($\Rightarrow$) Suppose that P_n is a ghost shape. If there exists any convex corner, say, $\boldsymbol{c} \in \angle Q \cap \bar{P}_n$ that is not a ghost corner. Then

$$(D(\boldsymbol{c}) \backslash (P_n \cup Q)) \cap R \neq \emptyset,$$

implying at least one of the two negative components of $D(\boldsymbol{c}) \backslash (P_n \cup Q)$ must be completely contained in some R_k with $k \geq 1$. Clearly $R_k \cup P_n$ is connected, and hence R_k and P_n belong to the same connected component of the illusory foreground $F = R \cup P$. This contradicts to the assumption that P_n alone is a ghost shape or a connected component of F. □

We believe that the framework in the current work may provide a novel track towards the final understanding of ghost shapes and dots, in particular, of the *transiency* nature of such illusory shapes. According to the characterizations just established above, we can say (i) that at the post fusion stage, each non-ghost convex corner provides an anchor or pinning point for stabilizing the perception of illusory shapes, and (ii) that a ghost shape could disappear sporadically due to lack of potential occluding areas and hence occluded shapes. The potential presence of occluded shapes can enhance the perception of illusory shapes against an otherwise featureless far background.

7 Conclusion

Inspired by perceptual evidences, we introduced a new class of visual cues called corner bases, which expand 0-dimensional corner points to localized 2-dimensional structures. A corner base can be considered as a degenerate T-junction where the far background and the foreground share the same surface color tone. To model the two fundamental factors driving human's illusory perception – closeness and alignment, we proposed to employ Euler's elastica as an effective tool to fuse or merge the scattered corner bases. The elastica fusion field naturally partitions the visual field into disjoint positive and negative components, which are then regrouped via a simple connectivity mechanism to form both the foreground illusory shapes and background occluded shapes.

While most existing models only compute the foreground illusory shapes, which are of the utmost interest, our model and method simultaneously construct a candidate for the background occluded shapes. With examples, we demonstrated that the illusory shapes and occluded shapes constructed by our model are consonant with human's illusory perception. Computationally, the elastica fusion energy has been implemented via its Γ-approximations, and robust and effective numerical schemes are designed for the 4th-order nonlinear PDE. Several numerical examples for generic configurations have been presented.

We also addressed the visual phenomenon of ghost shapes by developing proper definitions and characterization under our framework, and made a couple of conjectures regarding to the neurological foundations for the transiency associated with ghost shapes.

Compared with most existing works on variational illusory contours (VIC), our current work is essentially for variational illusory shapes (VIS). Assisted with the local cues of corner bases, the proposed model can be considered as a supervised VIS model, and thus has contributed a new dimension to the growing literature on illusory modeling.

References

[1] L. Ambrosio and V. M. Tortorelli. Approximation of functionals depending on jumps by elliptic functionals via Γ-convergence. *Comm. Pure Appl. Math.*, 43:999–1036, 1990.

[2] L. Ambrosio and V. M. Tortorelli. On the approximation of free discontinuity problems. *Boll. Un. Mat. Ital.*, 6-B:105–123, 1992.

[3] G. Aubert and P. Kornprobst. *Mathematical Problems in Image Processing*. Springer-Verlag, 2001.

[4] G. Aubert and L. Vese. A variational method in image recovery. *SIAM J. Numer. Anal.*, 34:1948–1979, 1997.

[5] G. Bellettini and R. March. Asymptotic properties of the Nitzberg-Mumford variational model for segmentation with depth. *International Series of Numerical Mathematics*, 154:75–84, 2006.

[6] J. W. Cahn and J. E. Hilliard. Free energy of a nonuniform system. I. Interfacial free energy. *J. Chem. Phys*, 28:258–267, 1958.

[7] T. F. Chan, S.-H. Kang, and J. Shen. Euler's elastica and curvature based inpainting. *SIAM J. Appl. Math.*, 63(2):564–592, 2002.

[8] T. F. Chan and J. Shen. Mathematical models for local nontexture inpaintings. *SIAM J. Appl. Math.*, 62(3):1019–1043, 2002.

[9] T. F. Chan and J. Shen. *Image Processing and Analysis: variational, PDE, wavelet, and stochastic methods*. SIAM Publisher, Philadelphia, 2005.

[10] T. F. Chan, J. Shen, and L. Vese. Variational PDE models in image processing. *Notices Amer. Math. Soc.*, 50:14–26, 2003.

[11] T. F. Chan and W. Zhu. Capture illusory contours: A level set based approach. *J. Math. Imaging Vis.*, 27:29–40, 2007.

[12] S. S. Chern, W. H. Chen, and K. S. Lam. *Lectures on Differential Geometry*. World Scientific, New Jersey, 1998.

[13] A. Coscia. On curvature sensitive image segmentation. *Nonlinear Analysis*, 39, 2000.

[14] G. Dal Maso. *An Introduction to* Γ*-Convergence*. Birkhauser, Boston, 1992.

[15] M. do Carmo. *Differential Geometry of Curves and Surfaces*. Prentice Hall, 1976.

[16] De Giorgi E. Some remarks on -convergence and least squares method. In Gianni Maso and GianFausto DellAntonio, editors, *Composite Media and Homogenization Theory*, volume 5 of *Progress in Nonlinear Differential Equations and Their Applications*, pages 135–142. Birkhuser Boston, 1991.

[17] S. Esedoglu and R. March. Segmentation with depth but without detecting junctions. *J. Math. Imaging Vision*, 18:7–15, 2003.

[18] L. C. Evans. *Partial Differential Equations*. Amer. Math. Soc., 1998.

[19] K. Fukushima. Neural network model for completing occluded contours. *Neural Networks*, 23:528–540, 2010.

[20] J. Geier, L. Sera, and L. Bernath. Stopping the Hermann grid illusion by simple sine distortion. *ECVP*, Abstracts, 2004.

[21] V. L. Ginzburg and L. D. Landau. On the theory of superconductivity. *Soviet Phys. JETP*, 20:1064–1082, 1950.

[22] G. H. Golub and C. F. Van Loan. *Matrix Computations*. The Johns Hopkins University Press, Baltimore, 1983.

[23] U. Grenander. *Lectures in Pattern Theory. I. II. and III.* Springer, 1976-1981.

[24] D. H. Grosof, R. M. Shapley, and M. J. Hawken. Macaque V1 neurons can signal illusory contours. *Nature*, 365:550–552, 1993.

[25] S. Grossberg and E. Mingolla. Neural dynamics of from perception: Boundary completion, illusory figures, and neon color spreading. *Psych. Rev.*, 92(2):173–211, 1985.

[26] F. Han and S.C. Zhu. Bottom-up/top-down image parsing with attribute graph grammars. *IEEE Trans. Pattern Anal. Machine Intelli.*, 31(1):59–73, 2009.

[27] L. Hermann. Eine erscheinung simultanen contrastes. *Pflügers Archiv für die gesamte Physiologie*, 3:13–15, 1870.

[28] Y.-M. Jung, S.-H. Kang, and J. Shen. Multiphase image segmentation by Modica-Mortola phase transition. *SIAM J. Appl. Math.*, 67(5):1213–1232, 2007.

[29] Y.-M. Jung and J. Shen. First-order modeling and stability analysis of illusory contours. *J. Visual Commun. Image Representation*, 19:42–55, 2008.

[30] D. J. Kalar, P. Garrigan, T. D. Wickens, J. D. Hilger, and P. J. Kellman. A unified model of illusory and occluded contour interpolation. *Vision Research*, 50:284–299, 2010.

[31] G. Kanizsa. *Organization in Vision*. Praeger, New York, 1979.

[32] D. C. Knill and W. Richards. *Perception as Bayesian Inference*. Cambridge Univ. Press, 1996.

[33] T. S. Lee and D. Mumford. Hierarchical Bayesian inference in the visual cortex. *J. Opt. Soc. Am. (A)*, 20(7):1434–1448, 2003.

[34] T. S. Lee and M. Nguyen. Dynamics of subjective contour formation in the early visual cortex. *Proc. Natl. Acad. Sci. U.S.A*, 98:1907–1911, 2001.

[35] J. Léveillé, M. Versace, and S. Grossberg. Running as fast as it can: How spiking dynamics form object groups in the laminar circuits of visual cortex. *J. Comput. Neurosci.*, 28:323–346, 2010.

[36] R. March. Visual reconstruction with discontinuities using variational methods. *Image Vision Comput.*, 10:30–38, 1992.

[37] R. March and M. Dozio. A variational method for the recovery of smooth boundaries. *Image Vision Comput.*, 15:705–712, 1997.

[38] S. Masnou and J.-M. Morel. Level-lines based disocclusion. *Proceedings of 5th IEEE Int'l Conf. on Image Process., Chicago*, 3:259–263, 1998.

[39] J. W. Milnor. *Topology from the Differentiable Viewpoint.* Princeton Univ. Press, revised edition, 1997.

[40] L. Modica. The gradient theory of phase-transitions and the minimal interface criterion. *Arch. Rational Mech. Anal.*, 98:123–142, 1987.

[41] L. Modica and S. Mortola. Un esempio di Gamma-convergenza. *Boll. Un. Mat. Ital. B*, 5-14(1):285–299, 1977.

[42] D. Mumford. Elastica and computer vision. In C. L. Bajaj, editor, *Algebraic Geometry and its Applications*, pages 491–506. Springer-Verlag, New York, 1994.

[43] D. Mumford. *Geometry Driven Diffusion in Computer Vision*, chapter "The Bayesian rationale for energy functionals", pages 141–153. Kluwer Academic, 1994.

[44] D. Mumford. Pattern theory: The mathematics of perception. *Int'l Congress Mathematicians (ICM)*, I, Beijing, 2002.

[45] M. M. Murray and C. S. Herrmann. Illusory contours: A window onto the neurophysiology of constructing perception. *Trends in Cognitive Sciences*, 17(9):471–481, 2013.

[46] M. Nitzberg, D. Mumford, and T. Shiota. *Filtering, Segmentation, and Depth.* Lecture Notes in Comp. Sci., Vol. 662. Springer-Verlag, Berlin, 1993.

[47] S. Osher and N. Paragios. *Geometric Level Set Methods in Imaging, Vision and Graphics.* Springer Verlag, 2002.

[48] S. J. Osher and R. P. Fedkiw. *Level Set Methods and Dynamic Implicit Surfaces.* Springer-Verlag, 2002.

[49] S. Petry and G. E. Meyer. *The perception of Illusory Contours.* Springer-Verlag, New York, 1987.

[50] A. Sarti, R. Malladi, and J. A. Sethian. Subjective surfaces: A geometric model for boundary completion. *Int'l J. Comp. Vision*, 46(3):201–221, 2002.

[51] J. A. Sethian. *Level Set Methods and Fast Marching Methods.* Cambridge University Press, 2nd edition, 1999.

[52] J. Shen. Inpainting and the fundamental problem of image processing. *SIAM News*, 36, 2003.

[53] J. Shen. Γ-convergence approximation to piecewise constant Mumford-Shah segmentation. *Lec. Notes Comp. Sci.*, 3708:499–506, 2005.

[54] J. Shen. A stochastic-variational model for soft Mumford-Shah segmentation. *Int'l J. Biomed. Imag.*, 2006(92329):1–14, 2006.

[55] L. Spillmann. The Hermann grid illusion: A tool for studying human perceptive field organization. *Perception*, 23:691708, 1994.

[56] D. A. Stanley and N. Rubin. fMRI activation in response to illusory contours and salient regions in the human lateral occipital complex. *Neuron*, 37:323–331, 2003.

[57] G. Strang. *Introduction to Linear Algebra*. Wellesley-Cambridge Press, 4th edition, 2009.

[58] A. N. Tikhonov. Regularization of incorrectly posed problems. *Soviet Math. Dokl.*, 4:1624–1627, 1963.

[59] L. A. Vese. A study in the BV space of a denoising-deblurring variational problem. *Appl. Math. Optim.*, 44(2):131–161, 2001.

[60] R. von der Heydt and E. Peterhans. Mechanism of contour perception in monkey visual cortex. I. Lines of pattern discontinuity. *J. Neurosci.*, 9:1731–1748, 1989.

[61] R. von der Heydt, E. Peterhans, and G. Baumgartner. Illusory contours and cortical neuron responses. *Science*, 224:1260–1262, 1984.

[62] T.F. Wu and S.C. Zhu. A numeric study of the bottom-up and top-down inference processes in and-or graphs. *Int'l J. Comput. Vision*, 93(2):226–252, 2011.

[63] X.-C.Tai, J. Hahn, and G. J. Chung. A fast algorithm for euler's elastica model using augmented lagrangian method. *SIAM Journal on Imaging Sciences*, 4(1):313–344, 2011.

[64] A. Yip and W. Zhu. A fast modified newtons method for curvature based denoising of 1d signals. *Inverse Problems and Imaging*, 7:1075 – 1097, 2013.

[65] A. Yoshino, M. Kawamoto, T. Yhoshida, N. Kobayashi, J. Shigemura, Y. Takahashi, and S. Nomura. Activation time course of responses to illusory contours and salient region: A high-density electrical mapping comparison. *Brain Research*, 1071:137–144, 2006.

[66] W. Zhu and T. Chan. Illusory contours using shape information. *UCLA CAM Tech. Report*, 03-09, 2005.

[67] W. Zhu, X.-C. Tai, and T. Chan. Augmented lagrangian method for a mean curvature based image denoising model. *Inverse Problems and Imaging*, 7:1409–1432, 2013.